

Cathodoluminescence Study of Micro-crack-induced Stress Relief for AlN Films on Si(111)

G. SARUSI,¹ O. MOSHE,¹ S. KHATSEVICH,¹ D.H. RICH,^{1,4} J. SALZMAN,² B. MEYLER,² M. SHANDALOV,³ and Y. GOLAN³

1.—Department of Physics, The Ilse Katz Center for Nano and Meso Scale Science and Technology, Ben-Gurion University of the Negev, P.O. Box 653, Beer-Sheva 84105, Israel. 2.—Department of Electrical Engineering, Solid State Institute and Microelectronic Center, Technion, Haifa 32000, Israel. 3.—Department of Materials Engineering, The Ilse Katz Center for Nano and Meso Scale Science and Technology, Ben-Gurion University of the Negev, P.O.B 653, Beer-Sheva 84105, Israel. 4.—E-mail: danrich@bgu.ac.il

Spatially, spectrally, and depth-resolved cathodoluminescence (CL) measurements were performed for high-quality thin AlN films grown on Si(111). CL spectra exhibited a sharp peak at 5.960 eV, corresponding to the near-band-edge excitonic emission of AlN. Depth-resolved CL analysis showed that deep level oxygen and carbon impurities are localized primarily at the AlN/Si interface and AlN outer surface. Monochromatic CL imaging of the near-band-edge emission exhibits a spotty pattern, which corresponds to high concentrations of threading dislocations and thermally induced microcracks in the thin layers. We have examined relief of the thermal stress in close proximity to single microcracks and intersecting microcracks. Local CL spectra acquired with a focused e-beam show blue-shifts as large as ~ 82 meV in the AlN near-band edge excitonic peaks, reflecting defect-induced reductions in the biaxial thermal stress, which has a maximum value of ~ 47 kbar.

Key words: AlN/Si heterostructures, III-nitride thin films, thermal stress, micro-cracks, cathodoluminescence

INTRODUCTION

AlN exhibits interesting physical properties (e.g., large bandgap, high-thermal conductivity, and large piezoelectricity) that are essential for applications in the ultraviolet wavelength range as well as for high-temperature electronic devices.^{1–4} Challenges in crystal growth due to the high-temperature growth requirement,^{5,6} dopant incorporation problems,⁷ and availability of suitable substrates for lattice-matching have limited the number of studies of AlN films.^{8,9} In this study, we have performed a detailed spatially and spectrally resolved cathodoluminescence (CL) study for high-quality thin AlN films grown on Si(111), which could serve as a practical and convenient substrate for future synthesis and processing of AlGaIn-based devices.^{10,11} Because of the large bandgap of ~ 6 eV for AlN, the high-energy and sharply focused electron beam (e-beam) employed in CL serves as an excellent probe for locally generating excess electrons and

holes and subsequently measuring variations in the luminescence efficiency caused by microcracks, dislocations, and impurities.¹² While the presence of thermal stress-induced microcracks is clearly undesirable when attempting to obtain high-quality thin film growth of III-nitride films on Si, the presence of cracking enables a study of the stress-induced energy shifts in the optical transitions that can be measured with a high-resolution spatially resolved probe, such as with CL. In this paper, we further attempt to show consistency between the deformation potentials determined by *ab initio* calculations, the measured energy shifts in the CL emission peaks at various positions near the microcracks, and the resulting values of uniaxial and biaxial stress near various crack configurations, as caused by the thermal expansion mismatch between Si and AlN.

EXPERIMENTAL

The AlN films were grown by low pressure organometallic vapor phase epitaxy. Use of Si(111)

further helped to minimize oxygen diffusion from the substrate, which occurs regularly when sapphire is used as the substrate.^{5,13} The growth temperature was $\sim 1100^\circ\text{C}$. The thickness of the resulting AlN films was $\sim 0.5\ \mu\text{m}$. The CL experiments were performed with a modified JEOL-5910 (Tokyo, Japan) scanning electron microscope (SEM) using variable beam currents (30 pA to 10 nA) and energies (3 keV to 15 keV). The luminescence was collected with a copper ellipsoidal mirror and transferred to a 1/4-m monochromator via a flexible solarization resistant ultraviolet optical fiber bundle that was designed for insertion into the SEM vacuum chamber. The dispersed light was detected with a multialkali photomultiplier tube, which enabled photon counting. The sample was cooled with a closed-cycle liquid He system connected to the SEM sample stage by a copper braid. The sample temperature was varied from 49 K to 300 K. The electron beam was rastered over a $64\ \mu\text{m} \times 48\ \mu\text{m}$ region during acquisition of CL spectra in the spatially integrated mode. Local CL spectra were also acquired by keeping the e-beam stationary and focused on specific features that will be discussed. Possible charging effects were examined by monitoring any changes in the apparent spatial resolution and distortions in the SEM imaging. At room temperature, we observed no change in the apparent spatial resolution and image quality for all e-beam currents (I_b) and energies (E_b) used in this study whereas a slight distortion of the SEM image was observed at $T = 49\ \text{K}$ when $E_b = 6\ \text{keV}$ and for $I_b > \sim 10\ \text{nA}$, indicative of the power dissipation conditions that can lead to charging of the sample.

RESULTS AND DISCUSSION

Spatially integrated CL spectra of the AlN sample at $T = 300\ \text{K}$ exhibit a sharp peak at 5.960 eV, as shown in Fig. 1a, corresponding to the near band-edge excitonic emission of AlN. Additional broader peaks were observed at 3.040 and 3.410 eV and were previously related to deep-level oxygen impurities.^{14–16} Two additional relatively small peaks were observed near 4.5 eV and are likely related to carbon impurities in AlN.^{1,14,15} This relatively weak emission demonstrates that only a minor carbon contamination occurred during sample growth.¹⁶

The depth-resolved analysis of the CL spectra shown in Fig. 1 was performed by varying the e-beam energy, E_b , which simultaneously changes the maximum depth R_m of e-beam penetration and position of maximal e-beam energy loss relative to the surface.¹⁷ The data shows that the peak CL emission ratio for the near-band edge of AlN relative to that for the deep-level oxygen emission at 3.040 and 3.410 eV [$I_{\text{AlN}}/I_{3.04}$ and $I_{\text{AlN}}/I_{3.41}$, respectively, in Fig. 1b] occurs for $E_b \approx 6\ \text{keV}$. This beam energy corresponds to $R_m \approx 170\ \text{nm}$, as calculated from the model of Everhart and Hoff.¹⁷ Thus $E_b \approx 6\ \text{keV}$ evidently corresponds to a condition that results in a peak in the electron-hole pair creation function near the center of the $0.5\text{-}\mu\text{m}$ -thick AlN film. Because the relative intensity of the deep-level emission is greatest when R_m corresponds to values in close proximity to either the AlN surface or the Si/AlN interface, we can infer that these defect- or impurity-related emissions originate mainly from such regions of the AlN film. Furthermore, the

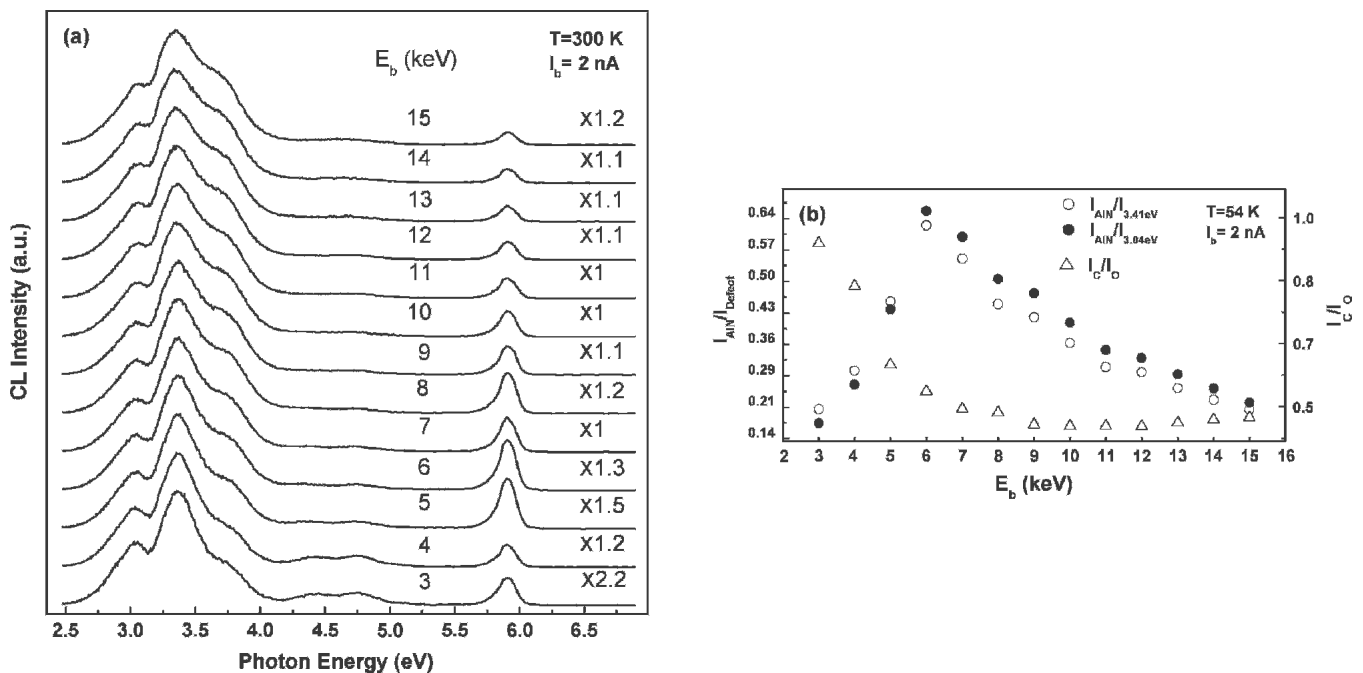


Fig. 1. Electron beam energy-dependent CL spectra showing the depth dependence of the emission in (a), while the ratios of the excitonic and impurity related peak emissions are shown as a function of beam energy (E_b) in (b). The ratio between the carbon related band and oxygen related band as a function of E_b is also shown in (b). The spectra were normalized to have nearly the same maximum CL intensity. The scale factors are indicated on the right.

intensity ratio between the deep-level oxygen and carbon emission [I_C/I_O in Fig. 1b] versus E_b reveals that the carbon incorporation is primarily at the AlN surface and to a lesser extent at the AlN/Si interface, as evidenced by the peaks in I_C/I_O at very low and high E_b .

To examine the dependence of the excitonic luminescence on varying excitation levels, CL spectra were acquired in the spatially integrated mode with the e-beam currents I_b , varying from 30 pA to 10 nA for $E_b = 6$ keV. The results in Fig. 2, for which the sample temperature was maintained at $T = 49$ K, reveal that the defect-related emission saturates at low beam currents whereas the excitonic emission increases almost linearly with beam current in this excitation range. The ratio of integrated intensities for the defect-related and exciton peaks versus I_b are shown in Fig. 2b and exhibits a nearly linear dependence for $I_b > \sim 5$ nA. This saturation behavior is consistent with the localization of oxygen impurities primarily at the AlN/Si interface and AlN surface. At very low excitations, carriers generated throughout the film will seek the lower energy defect channels through carrier diffusion toward the interface and surface. The gradual filling of the interface and surface defect levels will be followed by an increased relative rate of near-band edge electron-hole recombination, as evidenced by the increasing values of $I_{\text{AlN}}/I_{3.04}$ and $I_{\text{AlN}}/I_{3.41}$ for larger I_b in Fig. 2b.

SEM and monochromatic CL images of the near-band edge excitonic emission are shown in Fig. 3a–3d. The CL images in Fig. 3c and 3d were acquired at $h\nu = 5.96$ eV and exhibit a spotty emis-

sion pattern where defect-induced nonradiative recombination results in large spatial variations in the luminescence efficiency. Dark line defects (DLDs) observed in Fig. 3c and 3d appear in the CL images at the energy of the excitonic emission, indicating the presence of stress-induced microcracks running primarily along the high-symmetry wurtzite, $[11\bar{2}0]$, $[10\bar{1}0]$, and $[01\bar{1}0]$ directions. The transmission electron micrograph in Fig. 3e shows the single crystal nature of the AlN film and reveals in Fig. 3f clusters of threading dislocations that propagate from the AlN/Si interface to the surface.

The SEM images in Fig. 3a and 3b exhibit microcracks that intersect at angles of 60° and 120° , indicative of the hexagonal symmetry. Repeated temperature cycling of the sample between 300 K and 50 K increased the density of the microcracks and corresponding DLDs in the CL images. A biaxial tensile thermal stress is expected to form in the AlN layer during growth due to the large difference in the thermal expansion coefficient α between Si ($3 \times 10^{-6}/\text{K}$)¹⁸ and AlN ($7 \times 10^{-6}/\text{K}$).¹⁹ Interestingly, DLD-type features do not appear in the monochromatic CL images (not shown) for the broad oxygen-related peaks at 3.41 eV. This may relate to the localization of the oxygen impurity features of AlN at the lower AlN/Si interface where an incomplete severing of the AlN film may still result in an optically active AlN/Si interfacial region possessing sufficient oxygen impurities.

A further examination of local CL spectra acquired while the e-beam was focused on features observed in the CL images reveals a blue-shift in

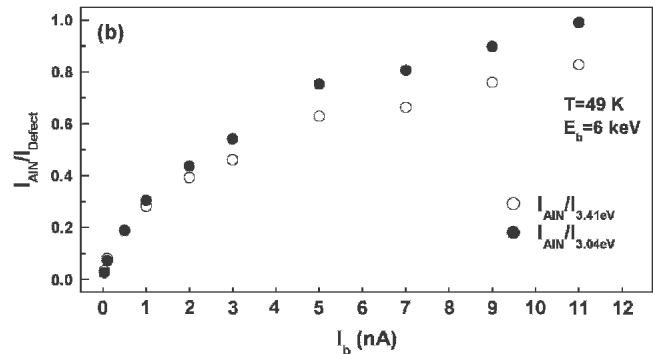
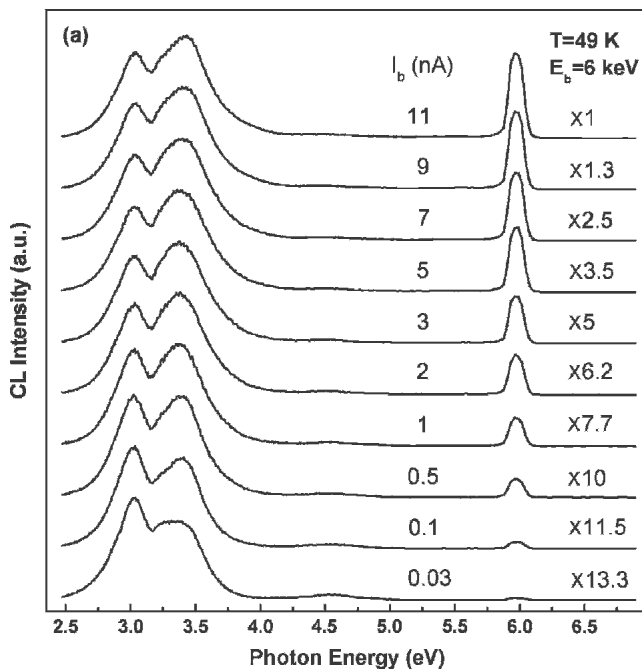


Fig. 2. Excitation-dependent CL spectra obtained for various beam currents (I_b) in (a) and the ratio of the intensities of the near-band edge to oxygen-impurity emissions I_{AlN}/I_O vs I_b in (b). The oxygen-related impurity emission saturates while the AlN near-band-edge emission increases nearly linearly as I_b increases. The spectra were normalized to have nearly the same maximum CL intensity. The scale factors are indicated on the right.

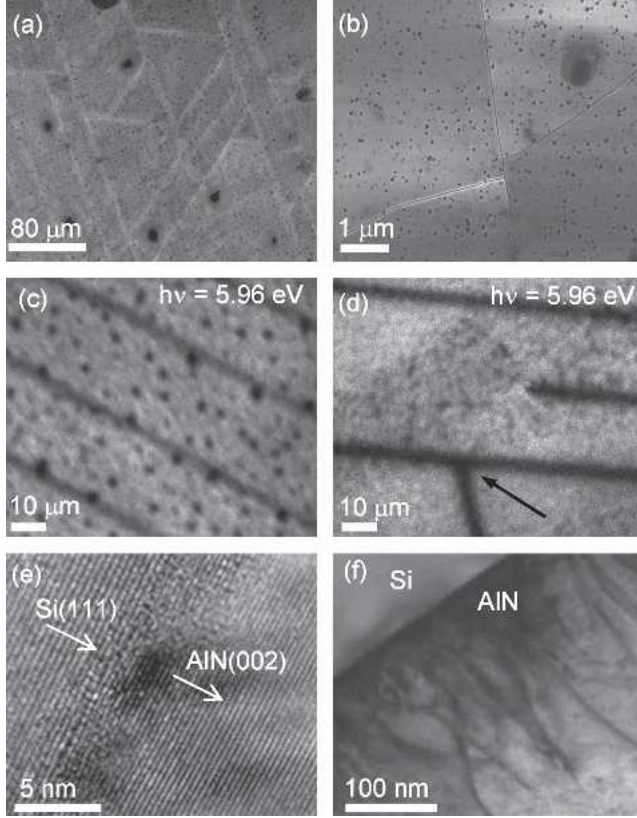


Fig. 3. SEM images in (a) and (b) showing the microcracks formed on the AlN film surface for different magnifications. Monochromatic CL images acquired for the AlN near-band-edge excitonic emission (5.96 eV) are shown in (c) and (d). A spotty emission pattern and a dark line defect (DLD) network that results from nonradiative recombination near the microcracks are observed. The arrow in (d) indicates a particular corner that was created by the intersection of two microcracks and was analyzed by local CL spectroscopy. The single-crystal nature of the film and the threading dislocations are shown in the TEM images of (e) and (f), respectively.

the near band-edge excitonic emission of ~ 6 meV and ~ 40 meV for dark spots and DLDs, respectively. Local CL spectroscopy with the e-beam focused on these features is shown in Fig. 4, revealing the excitonic peak positions of 5.997 eV, 6.003 eV, 6.040 eV, and 6.079 eV, for a bright region (reduced defects), dark spot (possibly dislocation clusters), single DLD (microcrack), and the corner of two intersecting DLDs, respectively. Dislocation clusters, as observed in the cross-sectional TEM image of Fig. 3f, likely give rise to the dark spots in the CL images of Fig. 3c and 3d, as has previously been observed in GaN.^{20,21} A considerable variation in the density of dark spots in the CL imaging of the AlN near-band-edge emission was observed throughout the sample, as demonstrated by the large variation in contrast observed between Fig. 3c and 3d. We deduce from this variation that the presence and density of dislocation clusters is also likely highly nonuniform throughout the sample. However, SEM imaging did not reveal contrast variations that correlated with the dark spots and dislocation clusters observed in the CL imaging of Fig. 3c and 3d. The relative blue-shift observed for dark

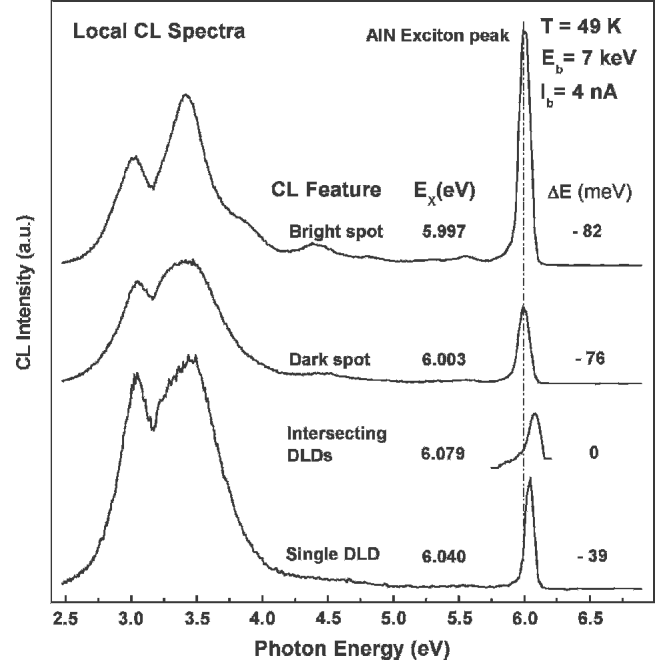


Fig. 4. Local CL spectra acquired with the e-beam focused in close proximity to various features that were observed in the CL imaging of Figs. 3(c) and 3(d). The four local CL spectra were acquired at a bright spot, dark spot, intersection of two DLDs (i.e., the corner of two microcracks, as shown in Fig. 3d), and a single DLD (microcrack). The relative shifts in the excitonic transition energy are also indicated and relate to the various stress configurations, as described in the text.

spots and DLDs in the peak of the excitonic luminescence is caused by a reduction in the thermal tensile stress of the AlN film created by these defects.

By assuming complete strain relief at the intersection of two microcracks or DLDs, the measured maximum blue-shift (82 meV from Fig. 4) in the near-band edge energy enables a quantitative estimation of the thermal stress in regions far from the microcracks. A diagonalization of the orbital-strain Hamiltonian for a wurtzite crystal permits a determination of the energy shift of the near-band edge excitonic emission as a function of the strain tensor ϵ_{ij} .^{22–24} For the present case of an AlN film, we use the appropriate strain and deformation potentials for this wurtzite structure.²⁵ For a diagonal strain tensor ϵ_{ij} (i.e., where $\epsilon_{ij} = 0$ for $i \neq j$), the energy of the near-band edge excitonic luminescence as a function of strain $E_X(\epsilon)$ is given by

$$E_X(\epsilon) = E_X(0) + a_1 \epsilon_{zz} + a_2 (\epsilon_{xx} + \epsilon_{yy}) + b_1 \epsilon_{zz} + b_2 (\epsilon_{xx} + \epsilon_{yy}) \quad (1)$$

where $E_X(0)$ represents the strain-free near-band edge excitonic transition energy of an AlN film, a_1 and a_2 are combined hydrostatic deformation potentials for electron-hole transitions across the bandgap, and b_1 and b_2 are uniaxial deformation potentials, which determine the relative splitting of the three top most valence bands for tensions or compressions parallel and perpendicular

to (0001).^{23–25} We have used the values of -3.39 , -11.81 , -9.42 , and $+4.02$ eV for a_1 , a_2 , b_1 , and b_2 , respectively, as determined by Wagner et al. through ab initio calculations for wurtzite AlN.²⁵ The intersection of two microcracks will provide a corner in which stress relief is nearly complete, thereby providing a reference for the measurement of $E_X(0)$ in a nearly unstrained ($\epsilon_{ii} \approx 0$) AlN region.^{26,27} A CL image of two intersecting DLDs whose corner was analyzed is shown in Fig. 3d.

For an in-plane biaxial tensile stress ($\sigma_{xx} = \sigma_{yy} = \tau_b$, $\sigma_{zz} = 0$), the strain components are given by $\epsilon_{xx} = \epsilon_{yy} = (C_{11} + C_{12} - 2C_{13}^2/C_{33})^{-1}\tau_b$ and $\epsilon_{zz} = (2C_{13}/C_{33})\epsilon_{xx}$,²⁵ where the elastic constants are given by Wright as $C_{11} = 3960$ kbar, $C_{12} = 1370$ kbar, $C_{13} = 1080$ kbar, and $C_{33} = 3730$ kbar.²⁸ τ_b represents the magnitude of the biaxial stress. Using Eq. 1, an in-plane biaxial stress yields an excitonic transition energy shift rate of $\Delta E/\tau_b = -1.735$ meV/kbar, where $\Delta E = E_X(\epsilon) - E_X(0)$. Using this rate, and the maximum shift of -82 meV between a bright region far from a DLD and the region of two intersecting DLDs, we estimate a biaxial stress $\tau_b \approx 47$ kbar. Similarly, an in-plane uniaxial stress ($\sigma_{xx} = \tau_u$, $\sigma_{yy} = \sigma_{zz} = 0$) gives rise to a shift of $\Delta E/\tau_u = -0.868$ meV/kbar, where τ_u represents the magnitude of the uniaxial stress. Thus, a shift of -39 meV between the two intersecting microcracks (an unstressed region) and a region in close proximity to the center of a DLD (Fig. 4) translates into a uniaxial stress $\tau_u \approx 45$ kbar near the center of the microcrack. Therefore, since $\tau_u \approx \tau_b$, we demonstrate consistency between the experimental results and the assumptions regarding stress relief near a single microcrack and two intersecting microcracks. Finally, we note that the 6-meV shift between the excitonic transitions in bright and dark regions (Fig. 4) is consistent with the presence of clusters of threading dislocations in dark regions, which partially relieve the biaxial stress and reduce the luminescence efficiency due to an increased rate of nonradiative recombination.

CONCLUSIONS

In conclusion, we have examined the optical properties of oxygen and carbon deep-level impurities in a thin AlN/Si(111) film with spatially, spectrally, and depth-resolved CL. We show that these impurities, in so far as their optical activity is concerned, are largely localized near the surface and AlN/Si interface. Thermal stress relief was examined by studying shifts in the excitonic energies near single and intersecting microcracks, which evidently give rise to uniaxial and unstressed configurations, respectively. Our analysis shows a maximum biaxial thermal stress of ~ 47 kbar at $T = 49$ K in relatively defect-free regions far from the microcracks.

ACKNOWLEDGEMENT

This work was supported in part by the Israel Science Foundation.

REFERENCES

1. K. Georgieva, G.K. Gueorguiev, R. Yakimova, and E. Janzen, *J. Appl. Phys.* 96, 9 (2004).
2. S.J. Pearton and C. Kuo, *MRS Bull.* 22, 17 (1997).
3. M.E. Levinshstein, S.L. Ramyantsev, and M.S. Shur, eds., *Properties of Advanced Semiconductor Materials* (New York: Wiley, 2001).
4. S. Strite and H. Morkoc, *J. Vac. Sci. Technol. B* 10, 1237 (1992).
5. J. Salzman, S. Praver, B. Meyler, Y. Golan, M. Shandalov, R. Sauer, and N. Teofilov, *Phys. Status Solidi C* 7, 2541 (2003).
6. Y. Ohba and R. Sato, *J. Cryst. Growth* 221, 258 (2000).
7. Y. Taniyasu, M. Kasu, and N. Kobayashi, *Appl. Phys. Lett.* 81, 1255 (2002).
8. A. Sarua, M. Kuball, and J.E. Van Nostrand, *Appl. Phys. Lett.* 81, 1426 (2002).
9. T. Prokofyeva, M. Seon, J. Vanbuskirk, M. Holtz, S.A. Nikishin, N.N. Faleev, H. Temkin, and S. Zollner, *Phys. Rev. B: Condens. Matter Mater. Phys.* 63, 125313 (2001).
10. A.T. Schremer, J.A. Smart, Y. Wang, O. Ambacher, N.C. Macdonald, and J.R. Shealy, *Appl. Phys. Lett.* 76, 736 (2000).
11. R. Behtash, H. Tobler, M. Neuburger, A. Schurr, H. Leier, Y. Cordier, F. Semond, F. Natali, and J. Massies, *IEEE Lett.* 39, 626 (2003).
12. For a review of the CL technique, see, e.g., B.G. Yacobi and D.B. Holt, *Cathodoluminescence Microscopy of Inorganic Solids* (New York: Plenum Press 1990).
13. A. Yoshida, *GaN and Related Semiconductors*, ed. J.H. Edgar, S. Strite, I. Akasaki, H. Amano, and C. Wetzel (London, UK: INSPEC IEEE, 1999).
14. J.A. Freitas, G.C.B. Braga, E. Silveira, J.G. Tischler, and M. Fatemi, *Appl. Phys. Lett.* 83, 13 (2003).
15. K.B. Nam, J. Li, M.L. Nakarmi, J.Y. Lin, and H.X. Jiang, *Appl. Phys. Lett.* 82, 1694 (2003).
16. J.L. Dupuie and E. Gulari, *Appl. Phys. Lett.* 59, 549 (1991).
17. T.E. Everhart and P.H. Hoff, *J. Appl. Phys.* 42, 5837 (1971).
18. J.H. Chae, J.Y. Lee, and S.W. Kang, *Sens. Actuators A* 75, 222 (1999).
19. K. Wang and R.R. Reeber, *Nitride Semiconductors*, ed. F.A. Ponce, S.P. DenBaars, B.K. Meyer, S. Nakamura, and S. Strite (Warrendale, PA: Mater. Res. Soc., 1997).
20. S.J. Rosner, G. Girolami, H. Marchand, P.T. Fini, J.P. Ibbetson, L. Zhao, S. Keller, U.K. Mishra, S.P. DenBaars, and J.S. Speck, *Appl. Phys. Lett.* 74, 2035 (1999).
21. H. Marchand, N. Zhang, L. Zhao, Y. Golan, S.J. Rosner, P.T. Fini, J.P. Ibbetson, S. Keller, J.S. Speck, S.P. DenBaars and U.K. Mishra, *MRS Internet J. Nitride Semicond. Res.* 4, (1999).
22. G. Pikus, *Zh. Eksp. Teor. Fiz.* 41, 1507 (1961); *Sov. Phys. JEPT* 14, 1075 (1962).
23. W. Shan, R.J. Hauenstein, A.J. Fischer, J.J. Song, W.G. Perry, M.D. Bresmer, R.F. Davis, and B. Goldenberg, *Phys. Rev. B: Condens. Matter Mater. Phys.* 54, 13460 (1996).
24. S.L. Chuang and C.S. Chang, *Semicond. Sci. Technol.* 12, 252 (1997).
25. J.M. Wagner and F. Bechstedt, *Phys. Status Solidi B* 234, 965 (2002).
26. D.H. Rich, A. Ksendzov, R.W. Terhune, F.J. Grunthaler, B.A. Wilson, H. Shen, M. Dutta, S.M. Vernon, and T.M. Dixon, *Phys. Rev. B: Condens. Matter Mater. Phys.* 43, 6836 (1991).
27. D. Rudloff et al., *Appl. Phys. Lett.* 82, 367 (2002).
28. I. Vurgaftman, J.R. Meyer, and L.R. Ram-Mohan, *J. Appl. Phys.* 89, 5815 (2001).